Available online at www.sciencedirect.com

SciVerse ScienceDirect

Ceramics International 39 (2013) 8213–8218

CERAMICS INTERNATIONAL

www.elsevier.com/locate/ceramint

Electrical conductivity of $SrBi_2Ta_2O_9$ ceramics

D. Kajewski*, Z. Ujma

Institute of Physics, University of Silesia, ul. Uniwersytecka 4, 40-007 Katowice, Poland

Received 10 December 2012; received in revised form 15 March 2013; accepted 2 April 2013
Available online 9 April 2013

Abstract

Aurivillius $SrBi_2Ta_2O_9$ (SBT) ceramics were prepared by applying the conventional solid state reaction method. The grain structure and stoichiometry were investigated with the use of a scanning electron microscope with an energy dispersion X-ray spectrometer (EDS). The X-ray diffraction studies revealed an orthorhombic structure with lattice parameters $a=5.486$ Å, $b=5.497$ Å and $c=24.91$ Å in the SBT. Dielectric properties were determined by impedance spectroscopy measurements. It was found that a strong low-frequency dielectric dispersion was present in this material. Its occurrence was ascribed to the presence of ionized space charge carriers such as oxygen vacancies. Dielectric relaxation was defined on the basis of an equivalent circuit. The temperature dependence of various electrical properties is described and discussed. The thermal activation energy for the grain electric conductivity was lower in the high temperature region ($T > 328.5$ °C, $E_{a-ht}=0.23$ eV) and higher in the low-temperature region ($T < 328.5$ °C, $E_{a-lt}=0.78$ eV). Moreover local conductivity measurements were performed with the use of the local conductive atomic force microscope method.

Keywords: C. Electrical conductivity; C. Impedance; D. Perovskites; D. Tantalates

1. Introduction

Bismuth layered structured ferroelectrics (BLSFs), particularly $SrBi_2Ta_2O_9$ (SBT), $SrBi_2Nb_2O_9$ (SBN) and their solid solution $SrBi_2(Nb_{1-x}Ta_x)_2O_9$ (SBNT), have attracted considerable scientific attention due to their fatigue-free properties that make them potentially suitable candidates for application in the FE-RAM [1]. Among these materials SBT exhibits both very good fatigue endurance as well as low switching voltage [2]. The layered structure of SBT allows for the interchange of Sr and Bi ions within the crystal lattice [3] which in consequence could lead to the local electrical heterogeneities as in the case of SBN [4]. Such heterogeneities could affect the ferroelectric properties as well as fatigue endurance. Therefore it is important to get a better insight into the electrical properties of SBT since they are not clear as yet.

In our recent works [4,5] we noticed a change in the activation energy of dc conductivity which was neither related to the ferroelectric phase transition in SBN nor $SrBi_2(Nb_{0.5}Ta_{0.5})_2O_9$, (SBNT 50/50). This change was ascribed to the existence of easy conductive paths. Their presence in SBN was first postulated by Palanduz et al. [6] and then observed for the first time by the authors in this material with the use of the local conductive atomic force microscopy (LC-AFM technique) [4]. The existence of such paths is possible since the cation exchange mentioned above may lead to a local formation of the Bi_2O_3–SrO double system within the crystallites. This system was widely investigated [7,8] and described as a good ionic conductor provided an adequate ratio of Sr–Bi is achieved and a proper number of oxygen vacancies is created. It is also worth stressing that oxygen vacancies are of significant importance in ferroelectric materials [9] since they can influence ferroelectric properties as well as play the role of nucleation centers.

On dealing with the Aurivillius phases such as SBN or SBT, where the cation exchange is possible, it is crucial that the mentioned heterogeneities should be taken into account. Several attempts have been made to understand the electrical behavior of SBT ceramics [9,10], however none of them have

*Corresponding author. Tel.: +48 32 3591134; fax: +48 32 2588431.
E-mail address: dariusz.kajewski@us.edu.pl (D. Kajewski).

0272-8842/$ - see front matter © 2013 Elsevier Ltd and Techna Group S.r.l. All rights reserved.
http://dx.doi.org/10.1016/j.ceramint.2013.04.005

considered these heterogeneities. Therefore, a consistent model of electrical conductivity in the SBN–SBT system has to be proposed.

The aim of this work is to present a consistent impedance analysis of SBT ceramics on the basis of the analysis given in the previous paper [4,5] as well as the local conductivity measurements which allow us to assign physical meaning to the equivalent electrical circuit elements. The other objective of this work is to propose a consistent model of electrical conductivity in SBN–SBT system.

2. Material and methods

The $SrBi_2Ta_2O_9$ ceramics were prepared by a standard mixed oxide method. The starting raw materials $SrCO_3$, Bi_2O_3 and Ta_2O_5 (all from Aldrich) were weighed and mixed together for 24 h. The mixtures were pressed into pellets and then sintered for 2 h at 950 °C inside a closed double crucible. The obtained substances were crushed, milled in a ball mill and sieved. The received powders were pressed again into pellets and sintered for 2 h at 1150 °C.

The grain structure and distribution of all components throughout the grains were examined by a SEM, JSM-5410, with an energy dispersion X-ray spectrometer (EDS) by Oxford Instruments. The crystal structure was analyzed by the X-ray diffraction (XRD, STADI diffractometer, Cu-K_α radiation). The density of the investigated ceramics was determined by the Archimedes displacement method with distilled water.

The obtained ceramics were used to measure the real (G) and the imaginary (B) parts of admittance (Y^*) as a function of frequency of the measuring field at a constant temperature in the frequency range from 5 Hz to 1 MHz. An automated measuring system with HP 4192A impedance analyzer was applied to measure and record G and B. All the ceramic pellets were polished to obtain flat and parallel surfaces and for electrical measurements their thickness was of about 0.5 mm. The samples were coated with silver electrodes using a silver paste without thermal treatment and de-aged at 500 °C for 10 min prior to measurements. Local conductivity measurements were performed with the use of an atomic force microscope-Jeol 4210 with a conductive cantilever. The metallographic specimen was applied for this measurement.

3. Theory

In our studies on SBN [4] and SBNT 50/50 [5] we proposed and applied the same mechanism of electrical conductivity. The mechanism was strictly connected with the existence of the $SrO–Bi_2O_3$ double system within those materials. Since the model does not include Nb or Ta ions, it is possible that it will apply to SBT ceramics as well. To check it we need to compare impedance spectra of SBT with the theoretical response of the postulated electrical equivalent circuit for SBN and SBT 50/50.

The equivalent circuit for SBN and SBNT 50/50 ceramics consists of two branches in the series (Fig. 1). The first branch

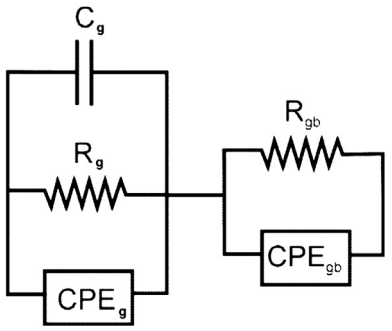

Fig. 1. Electrical equivalent circuit for the SBT ceramics.

represents intragranular properties and takes into account the dielectric as well as electric conductivity relaxations. The second branch corresponds to the grain boundary and electrode-interface effects, where R_{gb} and CPE_{gb} (Constant Phase Element) are parallel. Thus, the complex impedance (Z^*) in the case of such a circuit is expressed by the following equation:

$$Z^*(\omega) = Z_g^* + Z_{gb}^* \tag{1}$$

where

$$Z_g^* = \frac{R_g}{1 + C_g R_g j\omega + A_0 R_g (j\omega)^n} \tag{2}$$

and

$$Z_{gb}^* = \frac{R_{gb}}{1 + B_0 R_{gb} (j\omega)^m} \tag{3}$$

A_0, B_0, n and m are the temperature dependent parameters, $j = \sqrt{-1}$ and ω represent the angular frequency of the measuring field. Parameters n and m characterize the coupling between the charge carriers taking part in the polarization process-the lower the value, the stronger the ion–ion coupling [11]. The A_0 and B_0 parameters describe the contribution of the mechanism linking the universal Jonscher law to polarizability. To calculate all parameters, the fitting should be performed by using the complex nonlinear least-squares fitting [12] of both real and imaginary parts of the complex impedance (Eqs. (1)–(3)). Since we are interested in the electrical response of grains' interior, our further theoretical considerations will focus on the grain branch of the equivalent circuit.

From the equation

$$\frac{C^*}{C_0} = \frac{1}{j\omega C_0 Z^*} \tag{4}$$

where C^* is the complex capacitance and C_0 is the capacitance of the empty cell as well as from Eq. (2), one can calculate the normalized complex capacitance of grains

$$\frac{C^*}{C_0}(\omega) = \frac{C'}{C_0} - j\frac{C''}{C_0} = \frac{C_g}{C_0} + \frac{G_{DC}}{j\omega C_0} + \frac{A_0(T)}{C_0}(j\omega)^{n(T)-1} \tag{5}$$

where $G_{DC} = 1/R_g$ and C_g is the high frequency capacity of the grains' interior calculated from the equivalent circuit.

Hence the real (C'/C_0) and imaginary (C''/C_0) part can be calculated from the formulas

$$\frac{C'}{C_0} = \frac{C_g}{C_0} + \frac{A_0(T)}{C_0} sin\left(\frac{n(T)\pi}{2}\right)\omega^{n(T)-1} \quad (6)$$

$$\frac{C''}{C_0} = \frac{G_{DC}}{\omega C_0} + \frac{A_0(T)}{C_0} cos\left(\frac{n(T)\pi}{2}\right)\omega^{n(T)-1} \quad (7)$$

In the presented model the second part of Eqs. (6) and (7) describes the contribution of space charge carriers to the observed normalized capacitance of the sample. The first part of Eq. (7) gives the dc electric conductivity contribution to dielectric losses. Eqs. (6) and (7) allow to describe C'/C_0 and C''/C_0 both as a function of frequency and temperature. For low frequencies the second part of Eq. (6) responsible for the contribution of space charge carriers should become dominant whereas the contribution from C_g/C_0 should be negligible. Hence for constant n, the Eq. (6) should give a linear characteristic with a slope $n-1$ in $C'/C_0(\omega)$ on the log–log scale. The behavior of the imaginary part of the normalized capacitance in the low frequency region as well as in the high temperature should be explained by Eq. (7). In such conditions the dc electric conductivity contribution should be dominant and the slope of $C''/C_0(\omega)$ in log–log scale should be equal to -1.

In the chosen model, it is noteworthy that a change in the activation energy on the $\ln G_{DC}(1/T)$ plot also occurs at a temperature which is not associated with the para- to ferroelectric phase transition. An increase of temperature should result in the lowering of the activation energy which is related to the phase transition occurring in the Bi_2O_3–SrO double system [4,5,7,8,13] at about 300 °C.

4. Results and discussion

4.1. SEM and composition analysis

The observation of the microstructure of SBT ceramics revealed that the grains exhibited a plate-like shape with random orientation (Fig. 2). This is one of the characteristics of bismuth layered structured ferroelectrics. The plate thickness in the studied ceramics was of about 1 μm.

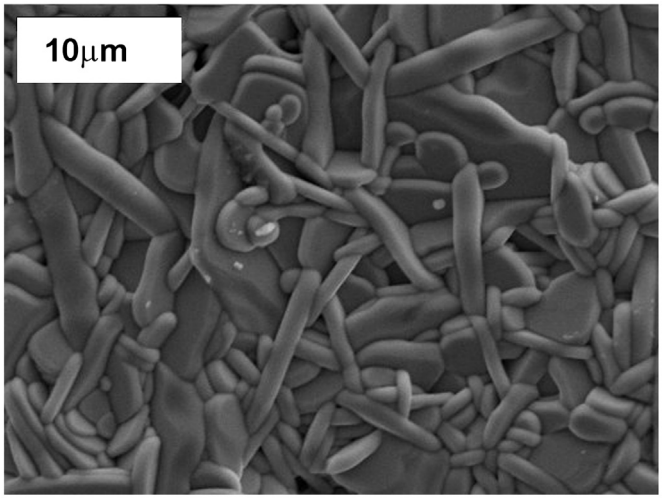

Fig. 2. SEM image of the free growth surface of the SBT specimen.

The homogeneous distribution of individual elements, apart from oxygen, within the grains of the ceramics was proved with the use of EDS. Moreover, the quantitative microanalysis performed by implementing the SEMQuant programs elaborated by Oxford Instruments showed that all samples had a stoichiometry close to the nominal one. The analysis of the amount of oxygen was conducted by the heat extraction method in helium atmosphere together with infrared spectroscopy. The concentration of oxygen was about 13.76 ± 0.14 mass%, which is less than the theoretical value of 14.24 mass%. Therefore, the existence of oxygen vacancies in the crystal lattice should be considered.

4.2. XRD analysis and density

The XRD patterns of SBT ceramics obtained at room temperature are shown in Fig. 3. The SBT sample exhibits an Aurivillius structure with no other phase present. We have confirmed the structure of our ceramics by fully indexing the observed peaks of the XRD spectrum according to the $A2_1am$ symmetry. The a and b lattice constants were determined with an error of ± 0.002 Å and their values equaled 5.486 Å and 5.497 Å, respectively. The c lattice constant was equal to about 24.91 ± 0.01 Å.

The calculations of the theoretical density were performed for comparison with the results obtained by the Archimedes method. The experimental density (6.7 g/cm^3) is about 93% of the theoretical one (7.25 g/cm^3) calculated from the XRD measurements. This difference is caused predominantly by pores.

4.3. Dielectric measurements

In Fig. 4 the real (Fig. 4a) and imaginary (Fig. 4b) parts of the normalized capacitance are presented as the function of frequency. In both cases, strong dispersion could be observed in the low-frequency range. With the decrease of temperature, a drop in dispersion was noticed. Dispersion exhibits linear changes on the log–log scale in the case of the normalized

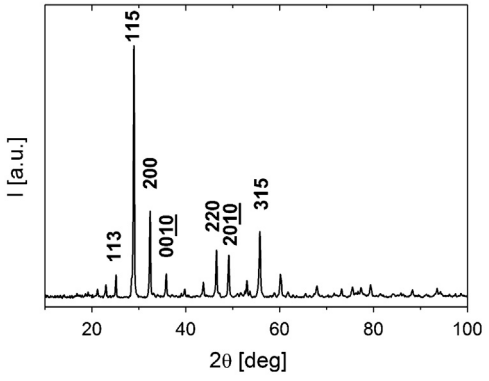

Fig. 3. Part of the diffraction patterns obtained at the room temperature of the $SrBi_2Ta_2O_9$ ceramics.

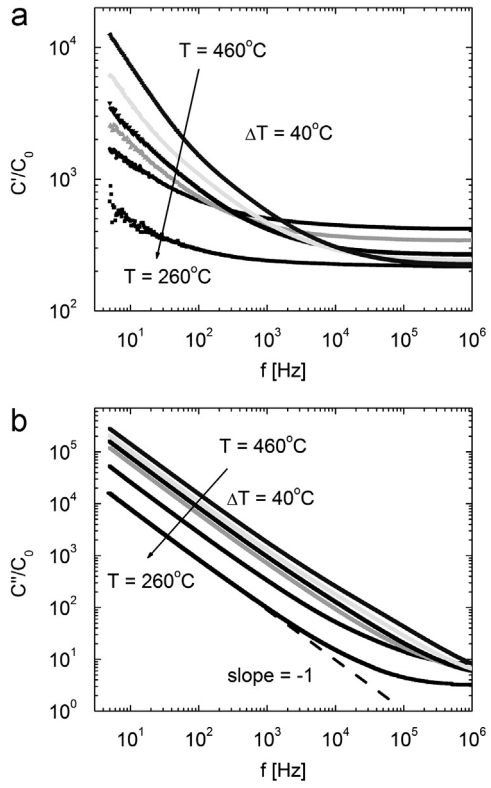

Fig. 4. The variations of real (a) and imaginary (b) part of normalized capacitance as a function of frequency at chosen temperatures.

C'/C_0 and C'/C_0. In the second case the slope was equal to about −1 (Fig. 4b). This suggests a strong coupling between the space charge carriers and the capacitance of the investigated samples. This effect fits the presented model of the electrical conductivity for these ceramics.

The obtained data of real part of admittance (G) were plotted as a function of frequency (Fig. 5). It allowed us to check the contribution of dc conductivity to the overall electrical response of the sample and to determine whether the changes of conductivity can be described by the universal Jonscher law. It can be seen that the plateau of conductivity, i.e. the frequency independent values of conductivity, corresponding to the dc conductivity, was observed in the low frequency region at high temperatures. In the higher frequency region, a strong dispersion of electric conductivity was noted and the changes of $G(f)$ in this region can be described as proportional to f^n, where f is the frequency of the measuring field and n is the parameter depending on temperature. The character of these changes does not depend on temperature. Nevertheless with the increase in temperature, it was noted that the range of frequency where the dispersion occurs moves to higher frequencies. Therefore it can be seen that the high frequency region can be described well by the universal Jonscher law. The same tendency was observed for SBN and for SBNT 50/50. It was also found that ac conductivity values decrease strongly with temperature below 330 °C in the whole frequency range. Such a big change in conductivity cannot be the effect of the para-to ferroelectric phase transition in SBT since it occurs at about 308 °C [14].

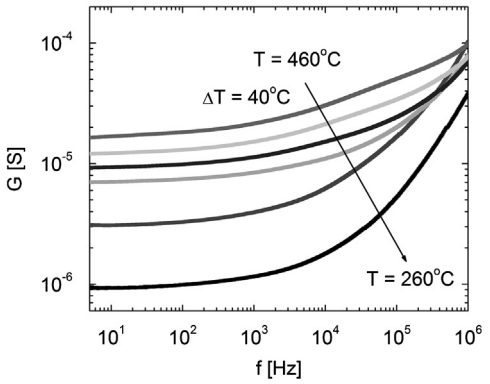

Fig. 5. Frequency dependence of real part of ac conductivity at various temperatures.

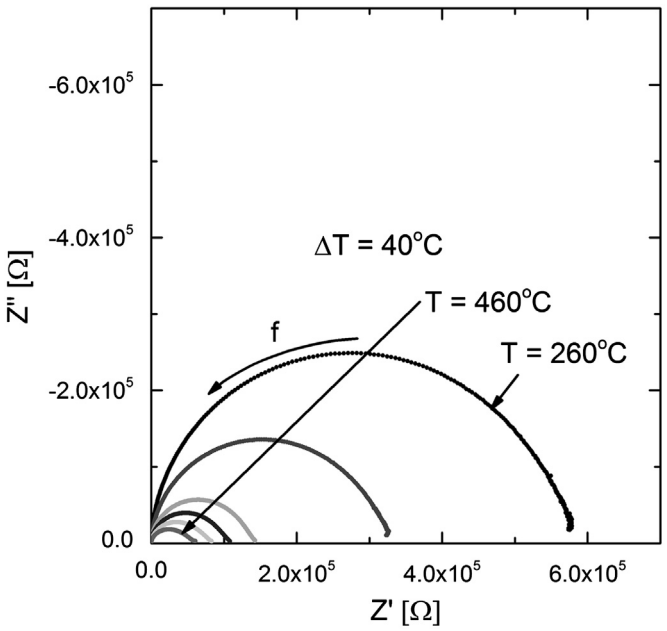

Fig. 6. Complex impedance plots at different temperatures.

From these observations it results that the electrical response of the sample fulfils the main assumptions of the proposed electrical equivalent circuit. To check whether the circuit fits the obtained response, a complex plot between the real and imaginary parts of impedance was drawn for selected temperatures. It is presented in Fig. 6. The obtained curves are neither semicircles nor circular arcs. In the high frequency region the Debye behavior was obeyed, where the angle between the tangent of the arc and the real axis was 90 °. Whereas in the part of the arc where $f \rightarrow 0$ the angle was less than 90 ° and temperature dependent. Such behavior was observed in SBN and SBNT 50/50. This suggests the presence of two different dispersion mechanisms in the sample. According to the above observation an equivalent circuit, shown in Fig. 1, could be applied with parameters fitting to the experimental data. The fitting error was about 1% in whole temperature and frequency range.

With the use of symbols from Eq. (5), it was possible to calculate the dc conductivity of the grain interior (G_{DC}).The

obtained results were in good agreement with the Arrhenius' formula, which indicates the thermal activation of the process (Fig. 7). The presence of two regions with different activation energies (E_a) was observed. In the range of lower temperatures $E_{a-lt}=0.78$ eV whereas in the range of higher temperatures $E_{a-ht}=0.23$ eV. The temperature at which the change in E_a occurred is equal to about $T_R=328.5$ °C. This temperature has no correlation with the ferroelectric phase transition temperature in this material.

The calculated changes of n and A_0 parameters with temperature are shown in Fig. 8.

The n parameter exhibits an almost constant behavior with the decrease of temperature down to T_R. Below T_R the parameter slightly increases with the decrease of temperature down to T_C. Below this temperature, the parameter remains constant. The A_0 parameter value decreases with the decrease of temperature revealing a small anomaly near T_R. Therefore it can be concluded that the contribution of space charge carriers is higher in elevated temperatures than in lower ones. This effect is responsible for the strong low frequency dispersion.

Temperature changes of the grain normalized capacitance (C_g/C_0) are presented in Fig. 9. This characteristic presents a typical maximum, correlated with the para- to ferroelectric phase transition. The temperature where the maximum of C_g/C_0 occurs remains in agreement with our previous observations [14].

On the basis of all the determined parameters, it was possible to calculate the contribution of space charge carriers to the normalized capacitance (C_{carr}/C_0) of the sample from the second part of Eq. (6). The temperature changes of C_{carr}/C_0 for the chosen frequencies are presented in Fig. 9.

For low frequencies the second part of Eq. (6), responsible for space charge carriers contribution, becomes dominant at higher temperatures whereas the contribution from C_g/C_0 is almost negligible. Hence the slope of C''/C_0(T) in the log–log scale is equal to −1 (Fig. 4b).

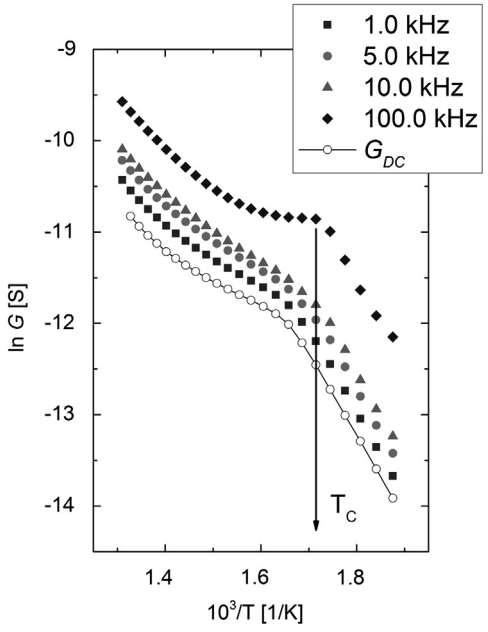

Fig. 7. Arrhenius plot of bulk (dc) and ac conductivity at different frequencies.

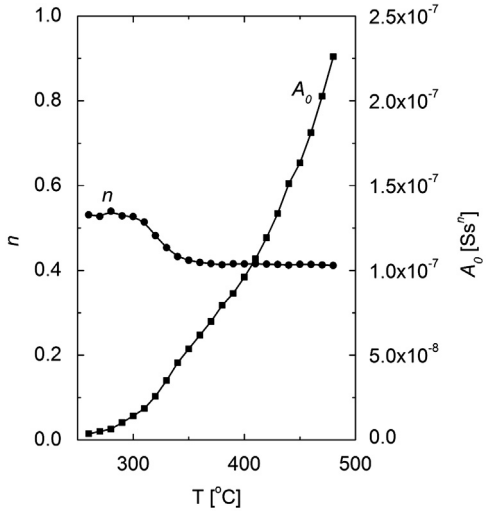

Fig. 8. Temperature dependence of the exponent n and prefactor A_0.

4.4. Local conductivity measurements

Local conductivity measurements at room temperature enabled us to obtain the topography (Fig. 10a) and the maps of local changes in resistivity (Fig. 10b). From the maps of resistivity, it can be seen that the electrical conductivity of the samples is highly heterogeneous and its changes by almost two orders of magnitude was observed. It is noteworthy that the investigated areas are situated within the grain interior and do not include the grain boundary which is clear from the simultaneous topography measurements. The areas of easy conductivity are not arranged in a regular way thus it can be

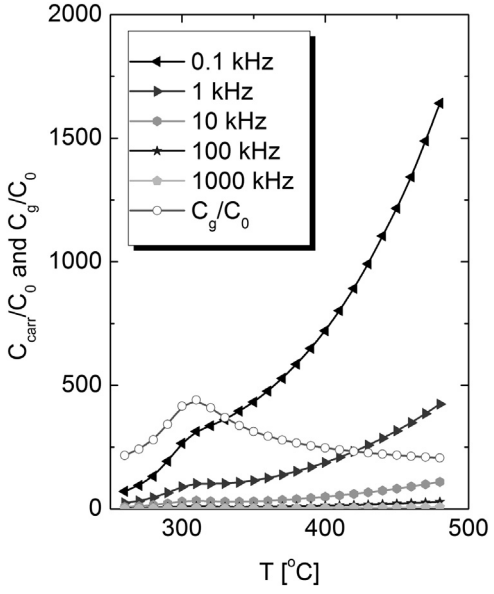

Fig. 9. The temperature dependence of grains' normalized capacitance and charge carrier-induced normalized capacitance for chosen frequencies.

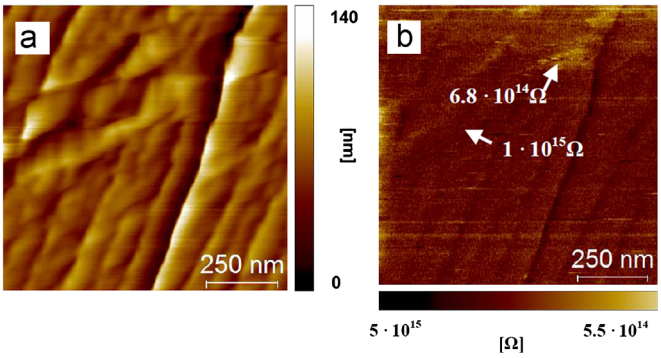

Fig. 10. Maps of topography (a) and local conductivity (b) changes of the SBT ceramics.

assumed that the easy conduction paths occur both in Bi_2O_2 slabs as well as in perovskite layers.

The character of the heterogeneity of electrical conductivity differs from that observed in $SrTiO_3$, where electrical conductivity appears along the oxygen dislocations. The area of these heterogeneities is about 2×2 nm^2 [15]. In the case of the studied ceramics the area of these heterogeneities is markedly larger, thus suggesting a high concentration of defects i.e. of oxygen vacancies caused by a different Sr/Bi ratio. Moreover the concentration regions of such defects do not cause a coherent diffraction visible in the XRD pattern. Moreover the local changes in the Sr/Bi ratio must also be smaller than the EDS analysis error which in our case was equal to about 0.1%. Hence they could not be detected by this method either.

On the basis of this observation, it can be assumed that the local character of electrical conductivity will determine the so-called macroscopic electrical conductivity.

5. Conclusions

On the basis of the above-mentioned analysis as well as our predictions we were able to choose the electrical equivalent circuit and construct the theory of easy conduction paths. The observation made allowed us to assume that in SBT ceramics easy conduction paths are formed due to cation exchange between Bi and Sr sub-lattices. Therefore the concentration of oxygen vacancies may vary, in consequence affecting the distribution of the relaxation times. This in turn could explain the significant temperature changes in ac conductivity and impedance.

Thus, the grain of such ceramics should be treated locally as a double Bi_2O_3–SrO system, which in literature is described as good ionic conductor provided the strontium-to-bismuth ratio is adequate. The change in the activation energy in the studied ceramics occurs since in the double Bi_2O_3–SrO system the structural phase transition appears on cooling from the higher to the lower electrically conducting structure [7,8].

Our work has also allowed us to form one consistent scenario of electrical conductivity in the studied group of materials from the Aurivillius' family, i.e. the SBN–SBT solid solution.

References

[1] C.A-Paz de Araujo, J.D. Cuchlaro, L.D. McMillan, M.C. Scott, J.F. Scott, Fatigue-free ferroelectric capacitors with platinum electrodes, Nature 374 (1995) 627–629.
[2] J.F. Scott, C.A. Araujo, Ferroelectric Memories, Science 246 (1989) 1400–1405.
[3] R. Macquart, B.J. Kennedy, Y. Shimakawa, Cation disorder in the ferroelectric oxides $ABi_2Ta_2O_9$, A=Ca, Sr, Ba, Journal of Solid State Chemistry 160 (2001) 174–177.
[4] D. Kajewski, Z. Ujma, Impedance analysis and local conductivity measurements of $SrBi_2Nb_2O_9$ ceramics, Phase Transitions 83 (2010) 897–908.
[5] D. Kajewski, Z. Ujma, Electrical properties of $SrBi_2(Nb_{0.5}Ta_{0.5})_2O_9$ ceramics, Journal of Physics and Chemistry of Solids 71 (2010) 24–29.
[6] A.C. Palanduz, D.M. Smyth, Defect chemistry and charge transport in $SrBi_2Nb_2O_9$, Journal of Electroceramics 11 (2003) 191–206.
[7] N.M. Sammes, G.A. Tompsett, H. Naefe, F. Aldinger, Bismuth based oxide electrolytes: structure and ionic conductivity, Journal of European Ceramic Society 19 (1999) 1801–1826.
[8] V.P. Zhereb, V.M. Skorikov, Metastable states in bismuth-containing oxide systems, Inorganic Materials 39 (2003) S121–S145.
[9] Yun Wu, Mike J. Forbess, Seana Seraji, Steven J. Limmer, Tammy P. Chou, Guozhong Cao, Impedance study of $SrBi_2Ta_2O_9$ and $SrBi_2(Ta_{0.9}V_{0.1})_2O_9$ Ferroelectrics, Materials Science and Engineering B86 (2001) 70–78.
[10] A.R. James, S. Balaji, S.B. Krupanidhi, Impedance-fatigue correlated studies on $SrBi_2Ta_2O_9$, Materials Science and Engineering B64 (1999) 149–156.
[11] K.S. Rao, D.M. Prasad, P.M. Krishna, B.H. Bindu, K. Suneetha, Frequency and temperature dependence of electrical properties of barium and gadolinium substituted $SrBi_2Nb_2O_9$ ceramics, Journal of Materials Science 42 (2007) 7363–7374.
[12] B.A. Boukamp, A linear Kronig–Kramers transform test for immittance data validation, Journal of the Electrochemical Society 142 (1995) 1885–1894.
[13] D. Kajewski, Z. Ujma, Impedance analysis of thermally modified $SrBi_2(Nb_{0.5}Ta_{0.5})_2O_9$ ceramics, Journal of Alloys and Compounds 509 (2011) 7532–7536.
[14] D. Kajewski, Z. Ujma, K. Szot, M. Pawelczyk, Dielectric properties and phase transition in $SrBi_2Nb_2O_9$–$SrBi_2Ta_2O_9$ solid solution, Ceramics International 35 (2009) 2351–2355.
[15] K. Szot, W. Speier, G. Bihlmayer, R. Waser, Nature Materials 5 (2006) 312–320.